OPEN ACCESS
IOP Publishing
Superconductor Science and Technology
Supercond. Sci. Technol. **36** (2023) 075001 (8pp)
https://doi.org/10.1088/1361-6668/acca50

Degradation of I_c due to residual stress in high-performance Nb_3Sn wires submitted to compressive transverse force

C Senatore[1,2,*], T Bagni[1], J Ferradas-Troitino[1,3], B Bordini[3] and A Ballarino[3]

[1] Department of Quantum Matter Physics, University of Geneva, Geneva, Switzerland
[2] Department of Nuclear and Particle Physics, University of Geneva, Geneva, Switzerland
[3] European Organization for Nuclear Research CERN, Geneva, Switzerland

E-mail: carmine.senatore@unige.ch

Received 1 February 2023, revised 17 March 2023
Accepted for publication 4 April 2023
Published 17 May 2023

Abstract

Future particle colliders in search for new physics at the energy frontier require the development of accelerator magnets capable of producing fields well beyond those attainable with Nb-Ti. As the next generation of high-field accelerator magnets is presently planned to be based on Nb_3Sn, it becomes crucial to establish precisely the mechanical limits at which this brittle and strain sensitive superconductor can operate safely. This paper reports on the stress dependence and the permanent reduction of the critical current under transverse compressive loads up to 240 MPa in state-of-the-art restacked-rod-process (RRP®) and powder-in-tube Nb_3Sn wires. Single-wire experiments were performed at 4.2 K in magnetic fields ranging between 16 T and 19 T on resin-impregnated samples to imitate the operating conditions of a wire in the Rutherford cable of an accelerator magnet. Depending on the wire technology, we measured irreversible stress limit values—defined as the transverse stress value, leading to a permanent reduction in the critical current of 5%, assessed by convention at 19 T—ranging between 110 MPa and 175 MPa. This permanent reduction of the critical current after mechanical unload can occur for two reasons, which can be concomitant: the plastic deformation of the Cu matrix that produces residual stresses on the Nb_3Sn lattice and the formation of cracks. We developed a method to identify the dominant degradation mechanism in our experiments that allowed us to predict the fraction of critical current lost due to residual stresses. Interestingly, we found that in the RRP® wires the measured reduction of I_c after unload from stresses as high as 240 MPa can be fully ascribed to residual stresses. An independent confirmation of this conclusion coming from a study combining x-ray tomography and deep learning Convolutional Neural Networks is also reported.

* Author to whom any correspondence should be addressed.

Keywords: Nb3Sn, electromechanical properties, accelerator magnets, FCC, critical current degradation, irreversible stress limit

(Some figures may appear in colour only in the online journal)

1. Introduction

The development of accelerator magnets that produce fields beyond those attained in the Large Hadron Collider (LHC) is among the key technologies required to expand the scientific reach of particle colliders in the search for new physics [1]. LHC, upgraded in luminosity with the ongoing high-luminosity LHC (HL-LHC) project, ready for beam commissioning in early 2029, will remain the most powerful accelerator in the world for at least the next two decades. This upgrade relies, among other innovative technologies, on cutting-edge quadrupole Nb_3Sn magnets reaching a peak field in the conductor of about 12 T [2]. After the latest update of the European Strategy for Particle Physics, released in June 2020 [3], and with the goal of increasing the potential to discover new particles and phenomena by pushing at the energy frontier, plans are going ahead to conceive a future proton–proton collider with a center-of-mass energy of at least 100 TeV, i.e. more than 7 times the design energy of the LHC. A first analysis of the general parameters of this 100 TeV Future Circular Collider (FCC) leads to a baseline configuration requiring dipole magnets of 16 T in a 100 km-long tunnel [1]. The above projects and studies are turning towards superconducting materials other than Nb-Ti, with Nb_3Sn being the preferred solution for magnetic fields of up to 16 T at present. A special grade Nb_3Sn wire was industrialized for HL-LHC, with values of the non-copper critical current density J_c, i.e. the critical current, I_c, divided by the wire cross-section area minus the Cu area, of at least 2450 A mm^{-2} at 4.2 K, 12 T, corresponding to about 1000 A mm^{-2} at 4.2 K, 16 T [4]. These values are about three times higher than those of the Nb_3Sn wires developed for the International Thermonuclear Experimental Reactor [5], but are still ∼40% below the performance requirement for the 16 T dipoles of the FCC [6]. Achieving the projected target of 1500 A mm^{-2} at 4.2 K, 16 T in a wire with proven scalability to long-length industrial production requires a major innovation step and this is the main drive of the Conductor Development Program launched by CERN in 2015 [7].

However, the superior superconducting properties of Nb_3Sn with respect to Nb-Ti are impaired by its mechanical fragility, which poses critical challenges to the magnet mechanics. As a result of the large fields and current densities, the superconducting coils of an accelerator magnet experience large electromagnetic forces. In dipoles, the azimuthal component of these forces accumulates at the midplane of the coil, with a magnitude of many hundreds kN m^{-1}. In the same way, the radial component pushes the coil outwards with a maximum displacement localized again at the midplane, while the axial component tends to elongate the coil. The mechanical design of the magnets aims to avoid deformation or movement of the conductor during powering, which may lead to premature quenches, and this is achieved by applying a mechanical pre-compression to the superconducting coils when assembling the magnet. However, the combination of pre-compression, thermal stresses during heat treatment and during the cooldown at cryogenic temperature, and electromagnetic forces arising in the operation regime exposes the brittle and strain sensitive Nb_3Sn to the risk of irreversible reduction of its critical current performance. Evidences of these permanent damages have been documented, for instance, for a two-in-one-aperture model dipole magnet wound with Nb_3Sn Rutherford cables, which was built in the frame of the HL-LHC project [8]. All four coils constituting the magnet exhibited a reduction in I_c distributed over a large fraction of the inner layer turn at the level of the midplane and it was suspected that degradation occurred due to too high levels of stress during the magnet's production.

Currently, a large majority of the proposed designs for the production of Nb_3Sn-based accelerator magnets entail peak stresses in the coils that are in the range of 150–200 MPa during magnet assembly and operation [9]. These peak stresses are compressive and act in the transverse direction of the Nb_3Sn Rutherford cables used to wind the coils. As the local stresses approach and, in some cases, exceed the currently understood limits of the conductor, it becomes crucial to establish precisely the mechanical limits to be adopted in any of the magnet assembly, cooling and operation phases. Hence, several laboratories have developed dedicated experiments aimed at testing the mechanical sensitivity of Nb_3Sn, in which a conductor—a full Rutherford cable, a sub-scale cable or a single wire—is exposed to mechanical loads relevant to accelerator magnet applications [10–17]. In particular, CERN has carried out extensive measurement campaigns on Rutherford cables to assess the effect of transverse loads exerted either at room temperature, to determine the maximum level of acceptable pre-compression during the magnet assembly process [11, 18, 19], or at 4.2 K to reproduce the electromagnetic forces acting on the coils at operating conditions [12, 13]. At the University of Geneva, we perform tests of the critical current on single Nb_3Sn wires submitted to transverse compressive loads at 4.2 K [17]. Wires are resin-impregnated to imitate the working conditions in the Rutherford cables of accelerator magnets [14–16]. During our experiments, samples are exposed to load/unload cycles at low temperature under increasing transverse stress values and this allows us to determine the reversible and irreversible components of the measured reduction of I_c. The reversible component is fully recovered when removing the load and is associated with the reversible reduction under stress of the upper critical field, B_{c2} [20]. On the other hand, two distinct mechanisms can contribute to the irreversible reduction of the critical current performance after unload: residual stresses and filament

breakages [13, 15, 19, 21]. First, the superconducting filaments in a Nb_3Sn wire are embedded in a soft Cu matrix, whose yield strength ranges between 40 MPa and ∼90 MPa [22, 23]. The plastic deformation of the Cu matrix determined by an external load imposes a residual stress to Nb_3Sn, after unload that in turn results in a reduction of B_{c2}. Second, Nb_3Sn is a brittle intermetallic compound characterized by a strong propensity to fracture. The formation of filament breakages at sufficiently high pressures leads to the reduction of the current carrying section of the wire.

In this paper, we report on the results of a measurement campaign of the critical current under transverse load in state-of-the-art restacked-rod-process (RRP®) and powder-in-tube (PIT) Nb_3Sn wires. We focused our study on wires extracted from production billets used at CERN for the development of magnets. In addition, we present here a method that allows us to identify the dominant mechanism behind the irreversible reduction of I_c and to quantify the fraction of I_c lost after unload due to residual stresses and filament breakages, respectively.

2. Sample characteristics and experimental details

Three Nb_3Sn wires have been studied in this work. Two of them are RRP® wires composed of 108 sub-elements embedded in a high-purity Cu matrix following the 108/127 hexagonal restack, with a nominal copper to non-copper ratio (Cu/non-Cu) equal to 1.2. They differ in diameter: the wire at 0.7 mm belongs to one of the production billets developed for the 11 T dipoles of HL-LHC [8], while that at 0.85 mm was extracted from a billet produced for use in the new interaction region quadrupoles of HL-LHC, identified by the acronym MQXF [24]. The third wire is a PIT wire with 192 filaments and a Cu/non-Cu volume ratio of approximately 1.22. It has a diameter of 1.0 mm and was produced for the FRESCA2 dipole project at CERN [25]. Dedicated measurement campaigns of the electromechanical properties of the RRP wire at 0.85 mm and of the PIT wire at 1.0 mm are reported in [16] and [15], respectively.

Technical parameters and main properties of the wires are resumed in table 1.

Wires were tested for the stress dependence of the critical current under transverse compressive load using a specially developed measurement device with a geometry similar to a Walters spring. The design and operation of the device are well documented in the literature [14–17, 21]. The wire sample is confined in a U-shaped groove, whose width, w, is adapted to the sample diameter: for the presented cases, it is $w = 1.0$ mm when the wire diameter is 0.7 mm and $w = 1.15$ mm when the wire diameter is 0.85 mm or 1.0 mm. A force of up to 35 kN is transmitted by an upper anvil that fits the groove. Samples are resin-impregnated to reproduce working conditions close to those of a Nb_3Sn wire in a Rutherford cable. Impregnation is performed using a de-gassed mixture of epoxy resin (type L + hardener L provided by R&G Faserverbundenwerkstoffe) and filler (thixotropic agent provided by SCS-Füllstoffe) in a 100:40:2 weight ratio. The choice of this type of impregnation relies on its favorable characteristics for manipulation and on its elastic modulus, which is very similar to the one of the CDT-101 K resin used for the impregnation of HL-LHC Nb_3Sn coils [26, 27].

Figure 1 shows the results of a typical I_c vs transverse stress measurement performed at $T = 4.2$ K on the RRP wire at 0.7 mm. I_c was measured at $B = 19$ T for increasing values of the applied transverse force and the stress on the wire was calculated as the force divided by the groove area. The force was increased in regular steps and in every other step the sample was fully unloaded to monitor the irreversible reduction of I_c. In addition, the magnetic field dependence of I_c under load and after unload was measured at given values of the applied force. The I_c values recorded for applied fields ranging between $B = 16$ T and $B = 19$ T were then used to determine the upper critical field, B_{c2}, via the well-known Kramer extrapolation [28]. No correction for the self-field generated by the current passing through the wire was applied. All I_c values reported in this paper have been determined with the 0.1 μV cm^{-1} criterion over a gauge length of 126 mm. The behavior of the wire in the field of interest for HL-LHC, i.e. at 12 T, could not be measured because of the high I_c values. However, the analysis reported in the following section provides a method to extrapolate to lower fields the results of the electromechanical tests.

3. Results and discussion

Figure 2 compares the evolution of the critical current under load and after unload for the three wires described in section 2, as measured at $B = 19$ T. The solid symbols show the dependence on the applied stress, σ, of the reduced $I_c{}^{load}$, i.e. I_c under load after normalization to the critical current at zero applied stress, I_{c0}. The open symbols represent the fraction of I_{c0} that is recovered after the release of the applied stress starting from the value corresponding to each point on the x-axis, i.e. $I_c{}^{unload}$ ($\sigma \rightarrow 0$) divided by I_{c0}. The examined wires exhibit a reduction of the critical current under transverse stress, which at $\sigma = 150$ MPa ranges between 20% and 50% with respect to I_{c0}. When the applied stress exceeds a certain threshold that is wire-dependent, a monotonic decrease of $I_c{}^{unload}$ ($\sigma \rightarrow 0$) is also observed, indicating a permanent reduction of the current carrying capability of the wire. By convention, we define as the irreversible stress limit, σ_{irr}, of the wire, the stress value leading to a reduction of $I_c{}^{unload}$ ($\sigma \rightarrow 0$) by 5% with respect to I_{c0}. The experiment revealed substantial differences in the value of σ_{irr} for the examined wires. We measured at 19 T $\sigma_{irr} = 155$ MPa for the RRP® wire at 0.70 mm, 175 MPa for the RRP® wire at 0.85 mm and 110 MPa for the PIT wire at 1.0 mm. There is a clear indication of a higher tolerance to transverse stress of RRP® wires compared to the PIT one, which is related to the differences in the internal architecture of the wire composites. In particular, the mechanical properties of the materials left at the center of the Nb_3Sn sub-elements or filaments after reaction are very different for RRP® and PIT wires and are expected to play a role in the electromechanical properties: the core of an RRP® sub-element consists

Table 1. Main characteristics of the investigated Nb_3Sn wires.

Technology	RRP®	RRP®	PIT
Billet ID	#073A02	#142A02	#31712
Wire diameter	0.70	0.85	1.0
Wire layout	108/127	108/127	192
Heat treatment schedule	210 C/48 h + 400 C/48 h + 650 C/50 h	210 °C/48 h + 400 °C/48 h + 665°C/50 h	620 °C/100 h + 640 °C/90 h
I_c (16 T,4.2 K) [A]	185	252	337
I_c (19 T, 4.2 K) [A]	67	112	164

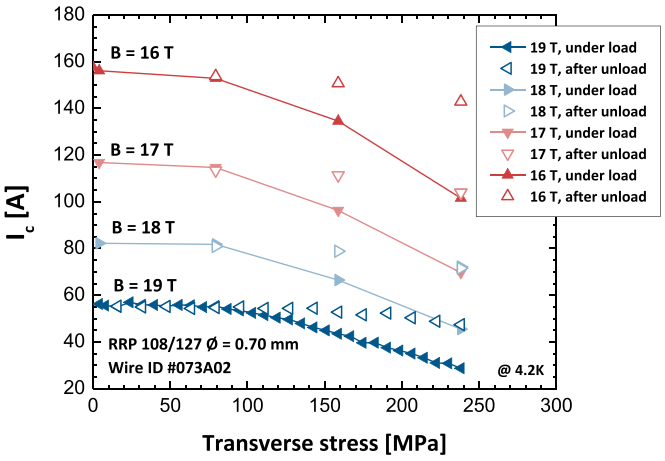

Figure 1. Dependence of the critical current I_c on the applied transverse stress for the 0.70 mm RRP wire impregnated with epoxy type L, at $T = 4.2$ K and $B = 16$ T, 17 T, 18 T and 19 T. Solid and open symbols correspond to the measurements under load and after unload, respectively.

of a solid low-Sn bronze matrix embedding a large number of micrometric voids [29], while the reacted filaments of PIT wires contain a poorly connected powder core where the reaction remainders are aggregated. Numerical simulations performed by Baffari and Bordini in [30] support also this conclusion. On the other hand, the difference in the σ_{irr} values of the two RRP® wires could be considered *a priori* an unexpected result, as the layout of their sub-elements is identical. The reduction of the transverse stress tolerance observed in the 0.70 mm wire may be influenced by the heat treatment schedule. Following the recipe used at CERN, the final step of the heat treatment for the 0.70 mm wire was performed at 650 °C for 50 h, i.e. at a lower temperature compared to the 665 °C used for the reaction of the 0.85 mm wire keeping the same duration. The lower temperature allows preserving a high residual resistivity ratio, RRR, of the Cu-matrix also in the smaller wire diameter, which is needed to ensure the stability of magnets against quenching. Nonetheless, a reduction of the electromechanical limits when decreasing the heat-treatment temperature was documented in the literature and confirmed in various wire designs of RRP® wires [31].

It was already pointed out in section 1 that the permanent reduction of the critical current observed when the load is removed occurs for two reasons, which can be concomitant: (a) the residual stress imposed to Nb_3Sn by the plastically-deformed Cu matrix and (b) the formation of cracks in the Nb_3Sn layer. Even if both mechanisms can lead to the irreversible reduction of I_c^{unload} ($\sigma \to 0$), their effects are expected to be different, as already pointed out in [15] and [13]. Similarly to what is observed when the wire is under load, the distortion of the Nb_3Sn lattice due to residual stress determines a reduction of the upper critical field after unload, B_{c2}^{unload} ($\sigma \to 0$), with respect to the value measured on the virgin wire, $B_{c2,0}$. On the other hand, when cracks are present in the Nb_3Sn layer, even if the critical current density of the superconductor is in principle preserved, the total current-carrying cross-section and, thus, I_c^{unload} ($\sigma \to 0$) can be reduced.

The following equation proposes an expression to describe the dependence of the critical current after stress release on the magnetic field, B, and on the maximum transverse stress applied to the wire, σ:

$$I_c^{unload}(B,\sigma \to 0) = f(\sigma \to 0)\, C \left[\frac{B_{c2}^{unload}(\sigma \to 0)}{B}\right]^{0.5} \times \left[1 - \frac{B}{B_{c2}^{unload}(\sigma \to 0)}\right]^{2}. \quad (1)$$

The magnetic field dependence follows the well-established scaling relation proposed in [32], with the constant prefactor C being independent of σ [13]. $f(\sigma \to 0)$ ranges between 0 and 1 and accounts for the reduction of the current-carrying cross-section due to cracks. It follows from (a) that the percentage of critical current drop due to cracks must be constant in field. The field dependence of I_c^{unload} ($\sigma \to 0$) is governed by B_{c2}^{unload} ($\sigma \to 0$). As the residual stresses on Nb_3Sn drive the reduction of B_{c2}^{unload} ($\sigma \to 0$), the percentage of critical current drop due to residual stresses increases with the applied field.

In figure 3 the stress dependence of the upper critical field under load, $B_{c2}^{load}(\sigma)$, and after unload, B_{c2}^{unload} ($\sigma \to 0$) for the three examined wires is reported. Following the same convention used in figure 2, each point of B_{c2}^{unload} ($\sigma \to 0$) is represented at the value of σ from which the unload started. The most important result of figure 3 is the continuous decrease of B_{c2}^{unload} ($\sigma \to 0$) after unload from increasing stress values. A reduction of more than 1 T with respect to $B_{c2,0}$ is measured after the last unload from 210 MPa in the PIT wire, while the final unload from 240 MPa leads to a drop of about 0.5 T for the two RRP wires. These experiments provide a clear indicator of the residual stresses acting on Nb_3Sn. However, this result is

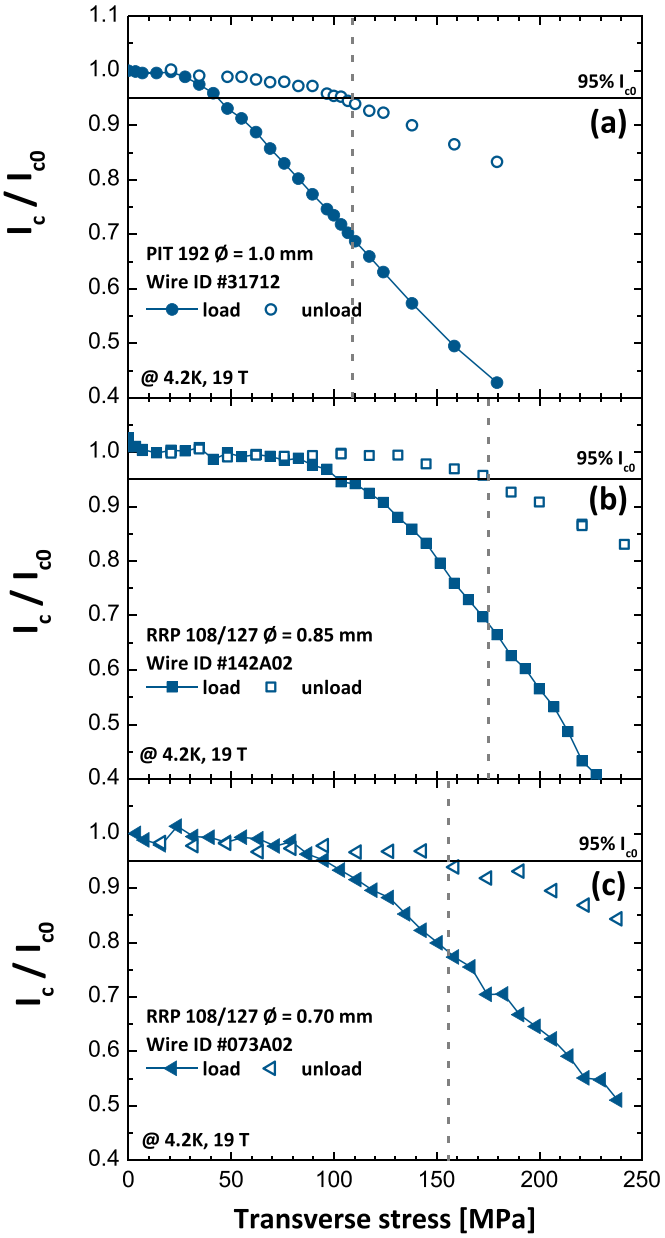

Figure 2. Dependence on the applied transverse stress at $T = 4.2$ K, $B = 19$ T of the critical current I_c normalized to the critical current at zero applied stress, I_{c0}, for (a) the 1 mm PIT wire, measured in a 1.15 mm wide groove; (b) the 0.85 mm RRP wire, measured in a 1.15 mm wide groove; (c) the 0.70 mm RRP wire, measured in a 1.0 mm wide groove. All wires were impregnated with epoxy type L. Solid and open symbols correspond to the measurements under load and after unload, respectively. Dashed lines indicate the conventionally defined irreversible stress limits.

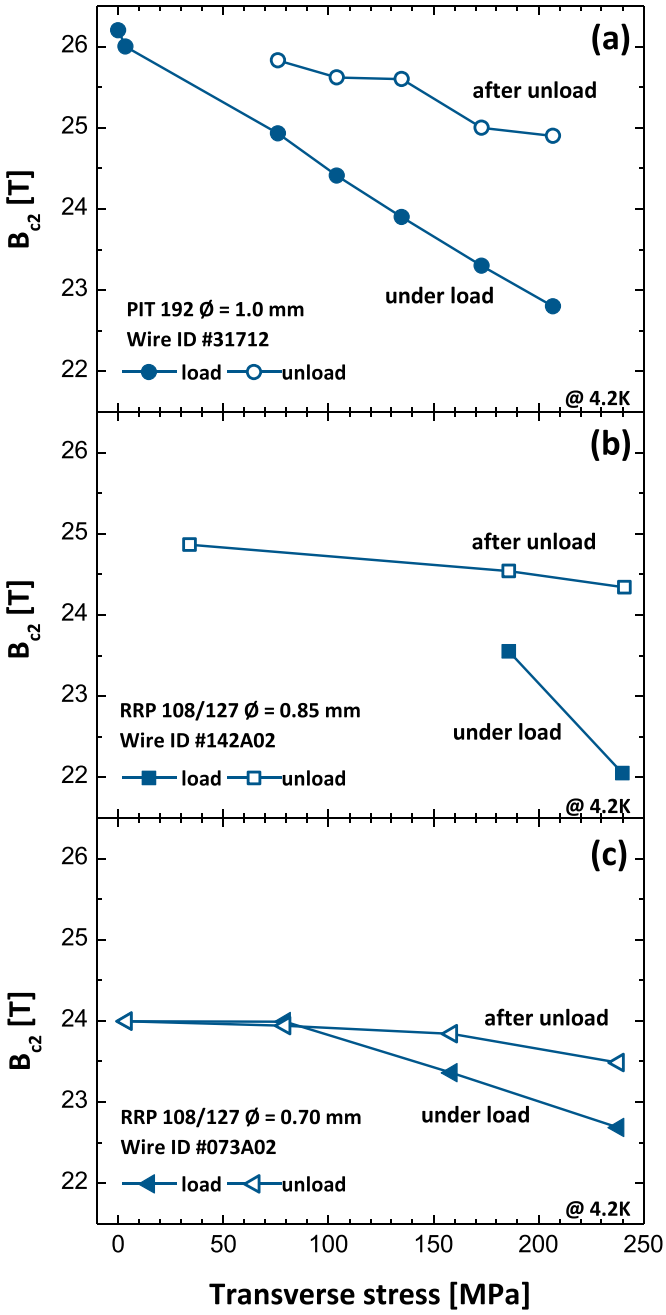

Figure 3. Upper critical field, B_{c2}, under load (solid symbols) and after unload (open symbols) as a function of the applied transverse stress for (a) the 1 mm PIT wire, measured in a 1.15 mm wide groove; (b) the 0.85 mm RRP wire, measured in a 1.15 mm wide groove; (c) the 0.70 mm RRP wire, measured in a 1.0 mm wide groove. B_{c2} values were determined using the I_c values recorded for applied fields between 16 T and 19 T, using the Kramer extrapolation [28]. The observed decrease of B_{c2} after unload from increasing stress values witnesses the presence of the residual stresses acting on Nb_3Sn.

not sufficient by itself to rule out the presence of cracks as a concomitant cause of the reduction of $I_c{}^{unload}$ $(\sigma \to 0)$. Introducing the measured values of $B_{c2}{}^{unload}$ $(\sigma \to 0)$ in equation (1) with $f(\sigma \to 0)$ fixed at 1, it is possible to calculate the expected percentage of critical current drop due to residual stress: any difference between the calculation and the $I_c{}^{unload}$ $(\sigma \to 0)/I_{c0}$ values reported in figure 2 can then be imputed to a reduction of the current-carrying cross-section due to cracks, i.e. to $f(\sigma \to 0) < 1$. The result of this comparison is shown in figure 4. For each of the three wire types, the solid stars were calculated with equation (1), using the $B_{c2}{}^{unload}$ $(\sigma \to 0)$ values in figure 3 and setting $f(\sigma \to 0) = 1$, with the error bars resulting from an indetermination of ± 0.1 T in the Kramer extrapolation for B_{c2}. The open symbols repropose the measured values of $I_c{}^{unload}$ $(\sigma \to 0)$ shown in figure 2.

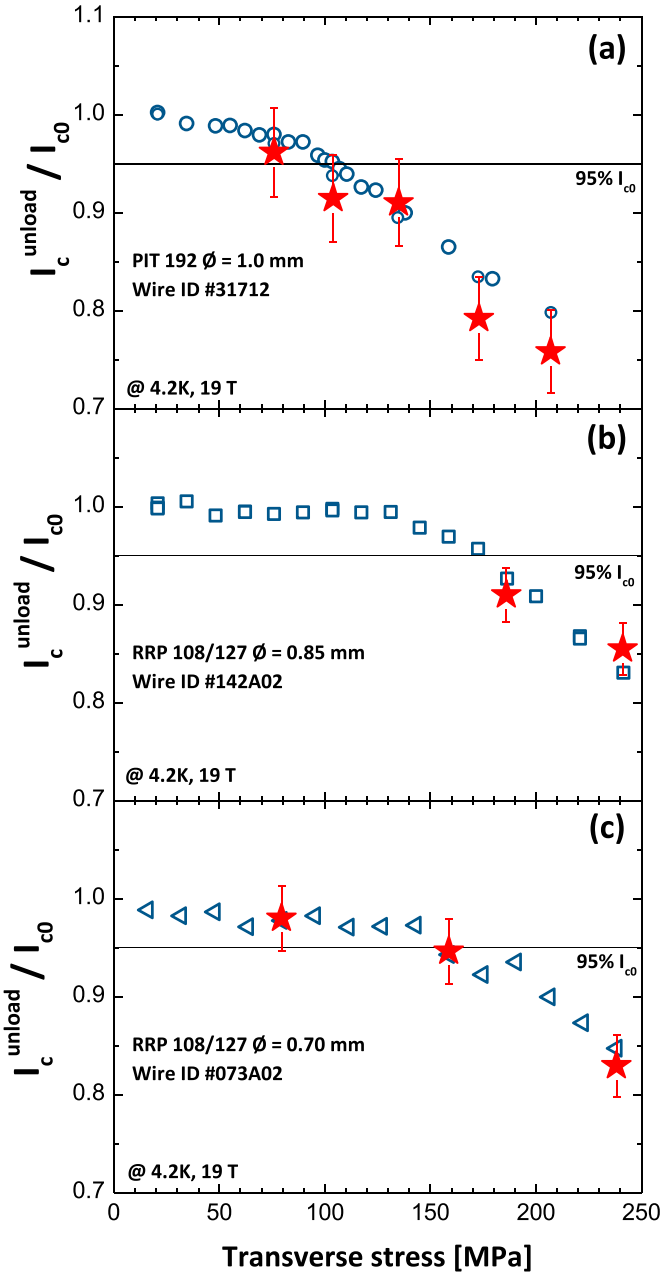

Figure 4. Evolution of the normalized critical current after unload, $I_c^{unload}(\sigma \to 0)/I_{c0}$, as a function of the applied transverse stress for (a) the 1 mm PIT wire, measured in a 1.15 mm wide groove; (b) the 0.85 mm RRP wire, measured in a 1.15 mm wide groove; (c) the 0.70 mm RRP wire, measured in a 1.0 mm wide groove. The solid stars represent the expected values of $I_c^{unload}(\sigma \to 0)/I_{c0}$ as predicted using the model in equation (1) and the measured values of B_{c2} after unload.

Very interestingly, the measured reduction of I_c^{unload} ($\sigma \to 0$) from stress values as high as 240 MPa can be fully accounted for with the reduction of B_{c2}^{unload} ($\sigma \to 0$) due to residual stress, regardless of the type of wire. Cracks and breakages in Nb_3Sn seem to have a negligible effect on the permanent degradation of the critical current in the geometry of our experiment, i.e. for an impregnated wire confined in a groove and submitted to transverse compressive load. Similar conclusions have been drawn by De Marzi *et al* [13] from the analysis of the critical current reduction under transverse stress of Rutherford cables based on the same type of PIT Nb_3Sn wires presented in this work.

An estimate of the residual stress values can be inferred by comparing the I_c data under load and after unload reported in figure 2. In particular, one can look for the values of applied stress that lead to the same I_c reduction measured after unload. The PIT wire exhibits an I_c value after the final unload from $\sigma_{unload} = 180$ MPa that matches the I_c value measured under load at $\sigma_{load} = 75$ MPa, whereas for the RRP wires, the I_c value after unload from $\sigma_{unload} = 240$ MPa corresponds to the I_c value measured under σ_{load} in the 135–145 MPa range. When the stress σ_{load} is applied to the wire, the resulting stress distribution on Nb_3Sn, which depends on the mechanical properties of the wire composite, leads to the same overall change in the superconducting properties as the residual stresses left after releasing σ_{unload}, even though the local stress distributions may differ. However, a mechanical analysis based on finite element simulations is required to extract a quantitative correlation between applied load, plastic deformation of the Cu matrix, and residual stress distribution in the Nb_3Sn phase. We plan to conduct such an analysis in future work. Notably, we observe that for both types of wires, the relative reduction of I_c remains consistent for a given difference in stress $\Delta\sigma = \sigma_{unload} - \sigma_{load}$, with I_c decreasing to approximately 83% of I_{c0} when $\Delta\sigma$ is approximately 100 MPa, and to 95% of I_{c0} when $\Delta\sigma$ is approximately 65 MPa.

An independent confirmation of the dominant role of residual stresses on the degradation of I_c came from a study combining x-ray tomography and deep learning Convolutional Neural Networks, reported in [33]. Tomography images were taken at the European Synchrotron Radiation Facility on the RRP wire sample at 0.7 mm extracted from the I_c vs transverse stress probe at the end of the experiment after the final unload from 240 MPa. Figure 5(a) shows a tomography cross section of the wire. Figure 5(b) provides a 3D perspective of the voids, which are formed during the reaction heat treatment, in cyan and of the cracks in yellow, as detected by deep learning. The wire volume examined by tomography corresponds to a scan length of about 1.5 mm. More details about the methods of detection and image recognition are reported in the [29, 33, 34]. Only very few cracks are present in the examined sample after unload from 240 MPa. These cracks are up to 30 μm long in the transverse direction, with a maximum width of $\sim$5 μm, while they propagate beyond the scan length of 1.5 mm in the longitudinal direction. However, none of the observed cracks creates interruptions in the subelements, which could lead to a reduction of the active cross-section. This observation supports the conclusion that the irreversible reduction under transverse compression of the critical current is only marginally influenced in our experiment by the presence of cracks. Other work also reports on micro-cracks, generated in the subelements of Nb_3Sn RRP® Rutherford cables subjected to transverse pressure at room temperature, which did not impact the measured critical current [18].

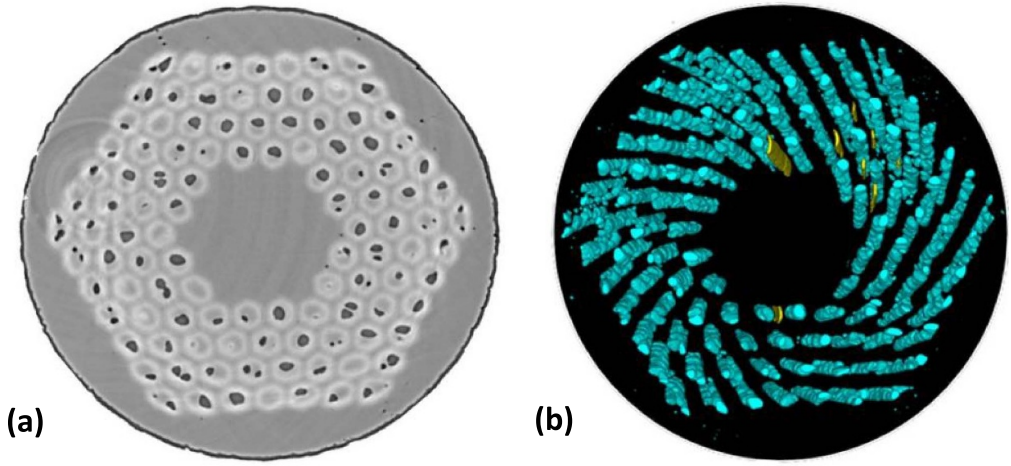

Figure 5. (a) Tomographic cross section of the 0.70 mm RRP wire after the final unload from 240 MPa, as measured at ESRF. (b) 3D reconstruction by Convolutional Neural Networks of the voids and cracks in the wire volume [33]. Voids are displayed in cyan, while cracks are shown in yellow.

4. Conclusions

This manuscript presents a comparison of the electromechanical response to transverse compressive loads of state-of-the-art Nb_3Sn wires produced by two different technologies, RRP® and PIT. The scope was to establish the limit of irreversible critical current degradation in wires used in high-field accelerator magnets, whose conductors are exposed to large mechanical loads during the assembly, cooling and operation phases. The experiments revealed marked differences in terms of tolerance to transverse stress between the measured RRP® and PIT wires, which follow from the different layout, composition and mechanical properties of the wire composites. The irreversible stress limit, defined as the stress level leading to a permanent reduction of the critical current by 5% at 19 T, was found to be 110 MPa for the PIT wire and in the 155–175 MPa range for the RRP® wires examined in this work. The degradation of I_c occurs generally from the combination of the effects of the residual stresses on Nb_3Sn, which result from a plastic deformation of the Cu matrix, and the formation of cracks. We developed a method to identify the dominant degradation mechanism following the evolution of the upper critical field after unload from increasing stress values. This analysis allowed us to conclude that the irreversible reduction of I_c measured in our experiments can be mainly ascribed to the effects of residual stresses. Complementary studies combining x-ray tomography and deep learning Convolutional Neural Networks were performed on the exact same samples tested for the I_c vs transverse stress dependence, after the final unload from 240 MPa. Interestingly, only very few cracks were detected in these samples exposed to very high stresses, and none of these cracks were creating interruptions to the flow of the current in the Nb_3Sn cross section. Therefore, this result provides an independent confirmation of our conclusions. The presented analyses and methodologies can be extended to evaluate the degradation mechanism of superconducting wires submitted to any type of mechanical load and suggest directions for the development of methods to enhance the mechanical limits of magnet conductors.

Data availability statement

The data that support the findings of this study are available upon reasonable request from the authors.

Acknowledgments

The authors acknowledge Mr Damien Zurmuehle for his technical assistance and Mr Francesco Lonardo for the valuable discussions. This work was performed under the auspices and with support from the Swiss Accelerator Research and Technology (CHART) program, https://chart.ch. Research supported by the European Organization for Nuclear Research (CERN), Memorandum of Understanding for the FCC Study, Addendum FCC-GOV-CC-0176 (KE 4612/ATS) and by the European Synchrotron Radiation Facility (Grant Nos. MA-4604).

ORCID iDs

C Senatore https://orcid.org/0000-0002-9191-5016
T Bagni https://orcid.org/0000-0001-8654-783X
J Ferradas-Troitino https://orcid.org/0000-0001-7874-9722

References

[1] Abada A *et al* 2019 FCC-hh: the Hadron Collider *Eur. Phys. J. Spec. Top.* **228** 755–1107
[2] Rossi L and Bruning O 2015 The high luminosity Large Hadron Collider *Advanced Series on Directions in High Energy Physics* vol 24 (Singapore: World Scientific)

[3] The European Strategy Group 2020 2020 update of the European strategy for particle physics *Technical Report* CERN-ESU-013

[4] Cooley L D, Ghosh A K, Dietderich D and Pong I 2017 Conductor specification and validation for high-luminosity *IEEE Trans. Appl. Supercond.* **27** 6000505

[5] Vostner A and Salpietro E 2005 The European Nb_3Sn advanced strand development programme *Fusion Eng. Des.* **75–79** 169–72

[6] Ballarino A and Bottura L 2015 Targets for R&D on Nb_3Sn conductor for high-energy physics *IEEE Trans. Appl. Supercond.* **25** 6000906

[7] Ballarino A *et al* 2019 The CERN FCC conductor development program: a worldwide effort for the future generation of high-field magnets *IEEE Trans. Appl. Supercond.* **29** 6001709

[8] Bordini B *et al* 2019 Nb_3Sn 11 T dipole for the high luminosity *Nb3Sn Accelerator Magnets* (Cham: Springer) pp 223–58

[9] Tommasini D *et al* 2017 The 16 T dipole development program for FCC *IEEE Trans. Appl. Supercond.* **27** 4000405

[10] Gao P, Dhallé M, Bordini B, Ballarino A and Ten Kate H H J 2020 Transverse-pressure susceptibility of high-Jc RRP and PIT types of Nb_3Sn Rutherford cables for accelerator magnets *Supercond. Sci. Technol.* **33** 125005

[11] Ebermann P *et al* 2018 Irreversible degradation of Nb_3Sn Rutherford cables due to transverse compressive stress at room temperature *Supercond. Sci. Technol.* **31** 065009

[12] Bordini B, Alknes P, Ballarino A, Bottura L and Oberli L 2014 Critical current measurements of high-Jc Nb_3Sn Rutherford cables under transverse compression *IEEE Trans. Appl. Supercond.* **24** 9501005

[13] De Marzi G, Bordini B and Baffari D 2021 On the mechanisms governing the critical current reduction in Nb_3Sn Rutherford cables under transverse stress *Sci. Rep.* **11** 7369

[14] Mondonico G, Seeber B, Ferreira A, Bordini B, Oberli L, Bottura L, Ballarino A, Flükiger R and Senatore C 2012 Effect of quasi-hydrostatical radial pressure on Ic of Nb_3Sn wires *Supercond. Sci. Technol.* **25** 115002

[15] Gamperle L, Ferradas J, Barth C, Bordini B, Tommasini D and Senatore C 2020 Determination of the electromechanical limits under transverse stress of high-performance Nb_3Sn Rutherford cables from a single-wire experiment *Phys. Rev. Res.* **2** 013211

[16] Ferradas Troitino J, Bagni T, Barth C, Bordini B, Ferracin P, Gamperle L, Tommasini D, Zurmuehle D and Senatore C 2021 Effects of the initial axial strain state on the response to transverse stress of high-performance RRP Nb_3Sn wires *Supercond. Sci. Technol.* **34** 035008

[17] Seeber B, Ferreira A, Abacherli V, Boutboul T, Oberli L and Flukiger R 2007 Transport properties up to 1000 A of Nb_3Sn wires under transverse compressive stress *IEEE Trans. Appl. Supercond.* **17** 2642

[18] Lenoir G 2022 Effect of transverse compressive stress on Nb_3Sn Rutherford cables for accelerator magnets (available at: https://indico.cern.ch/event/1138737/)

[19] Puthran K, Barth C, Ballarino A, Devred A and Arndt T 2023 Onset of mechanical degradation due to transverse compressive stress in Nb_3Sn Rutherford-type cables *IEEE Trans. Appl. Supercond.* **33** 8400406

[20] ten Haken B, Godeke A and ten Kate H H J 1999 The strain dependence of the critical properties of Nb_3Sn conductors *J. Appl. Phys.* **85** 3247

[21] Calzolaio C, Mondonico G, Ballarino A, Bordini B, Bottura L, Oberli L and Senatore C 2015 Electro-mechanical properties of PIT Nb_3Sn wires under transverse stress: experimental results and FEM analysis *Supercond. Sci. Technol.* **28** 055014

[22] Vallone G, Bordini B and Ferracin P 2018 Computation of the reversible critical current degradation in Nb_3Sn Rutherford cables for particle accelerator magnets *IEEE Trans. Appl. Supercond.* **28** 4801506

[23] Mitchell N 2005 Finite element simulations of elasto-plastic processes *Cryogenics* **45** 501–15

[24] Ferracin P *et al* 2015 Development of MQXF: the Nb_3Sn low-β quadrupole for the HiLumi LHC *IEEE Trans. Appl. Supercond.* **26** 4000207

[25] Bordini B, Bottura L, Mondonico G, Oberli L, Richter D, Seeber B, Senatore C, Takala E and Valentinis D 2012 Extensive characterization of the 1 mm PIT Nb_3Sn strand for the 13-T FRESCA2 magnet *IEEE Trans. Appl. Supercond.* **22** 6000304

[26] Meyer M 2018 Mechanical characterization of CTD 101K and, CERN *EDMS* **v1** 1890057

[27] Crouvizier M 2018 Impregnated epoxy flexural tests, CERN *EDMS* **v1** 1902476

[28] Kramer E J 1973 Scaling laws for flux pinning in hard superconductors *J. Appl. Phys.* **44** 1360–70

[29] Bagni T, Bovone G, Rack A, Mauro D, Barth C, Matera D, Buta F and Senatore C 2021 Machine learning applied to x-ray tomography as a new tool to analyze the voids in RRP Nb_3Sn wires *Sci. Rep.* **11** 7767

[30] Baffari D and Bordini B 2022 Effect of the sub-elements layout on the electro-mechanical properties of high Jc Nb_3Sn wires under transverse load: numerical simulations *IEEE Trans. Appl. Supercond.* **36** 6001306

[31] Cheggour N, Stauffer T C, Starch W, Lee P J, Splett J D, Goodrich L F and Ghosh A K 2018 Precipitous change of the irreversible strain limit with heat-treatment temperature in Nb_3Sn wires made by the restacked-rod process *Sci. Rep.* **8** 13048

[32] Ekin J W 2010 Unified scaling law for flux pinning in practical superconductors: i. Separability postulate, raw scaling data and parameterization at moderate strains *Supercond. Sci. Technol.* **23** 083001

[33] Bagni T, Mauro D, Majkut M, Rack A and Senatore C 2022 Formation and propagation of cracks in RRP Nb_3Sn wires studied by deep learning applied to x-ray tomography *Supercond. Sci. Technol.* **35** 104003

[34] Bagni T, Haldi H, Mauro D and Senatore C 2022 Tomography analysis tool: an application for image analysis based on unsupervised machine learning *IOP SciNotes* **3** 015201